RSC Advances

ROYAL SOCIETY OF CHEMISTRY

PAPER

View Article Online
View Journal | View Issue

Cite this: *RSC Adv.*, 2024, **14**, 8322

Heterocyclic (pyrazine)carboxamide Ru(II) complexes: structural, experimental and theoretical studies of interactions with biomolecules and cytotoxicity†

Nokwanda Tsaulwayo,[a] Reinner O. Omondi, ‡[a] Paranthaman Vijayan, [a] Nicole R. S. Sibuyi, [b] Miché D. Meyer,[b] Mervin Meyer[b] and Stephen O. Ojwach *[a]

Received 20th January 2024
Accepted 5th March 2024

DOI: 10.1039/d4ra00525b

rsc.li/rsc-advances

Treatments of *N*-(1*H*-benzo[*d*]imidazol-2-yl)pyrazine-2-carboxamide (**HL$_1$**) and *N*-(benzo[*d*]thiazol-2-yl) pyrazine-2-carboxamide carboxamide ligands (**HL$_2$**) with [Ru(*p*-cymene)Cl$_2$]$_2$ and [Ru(PPh$_3$)$_3$Cl$_2$] precursors afforded the respective Ru(II) complexes [Ru(L$_1$)(*p*-cymene)Cl] (**Ru1**), [Ru(L$_2$)(*p*-cymene)Cl] (**Ru2**), [Ru(L$_1$)(PPh$_3$)$_2$Cl] (**Ru3**), and [Ru(L$_2$)(PPh$_3$)$_2$Cl] (**Ru4**). These complexes were characterized by NMR, FT-IR spectroscopies, mass spectrometry, elemental analyses, and crystal X-ray crystallography for **Ru2**. The molecular structure of complex **Ru2** contains one mono-anionic bidentate bound ligand and display pseudo-octahedral piano stool geometry around the Ru(II) atom. The interactions with calf thymus DNA (CT-DNA) and bovine serum albumin (BSA) were investigated by spectroscopic techniques. The experimental binding studies suggest that complexes **Ru1–Ru4** interact with DNA, primarily through minor groove binding, as supported by molecular docking results. Additionally, these complexes exhibit strong quenching of the fluorescence of tryptophan residues in BSA, displaying static quenching. The *in vitro* cytotoxicity studies of compounds **Ru1–Ru4** were assessed in cancer cell lines (A549, PC-3, HT-29, Caco-2, and HeLa), as well as a non-cancer line (KMST-6). Compounds **Ru1** and **Ru2** exhibited superior cytotoxicity compared to **Ru3** and **Ru4**. The *in vitro* cytotoxicity and selectivity of compounds **Ru1** and **Ru2** against A549, PC-3, and Caco-2 cell lines surpassed that of cisplatin.

Introduction

Since the discovery of cisplatin in cancer therapy, research into metal-based chemotherapeutic agents has gained momentum.[1–4] This endeavour is underpinned by the dual objectives of enhancing cytotoxicity against malignant cells, while concurrently striving to limit the side effects of these chemotherapeutic drugs.[5–10] Among the numerous classes of metal complexes being investigated for their potential cancer therapy, ruthenium(II) complexes have emerged as a popular choice for non-platinum(II) based drugs. This is largely due to their desirable rate of ligand substitution kinetics, which are amenable to the dynamics observed in cellular processes, and thereby minimizing undesirable side reactions.[11,12] Furthermore Ru(II) complexes have the ability to mimic iron in their interaction with serum transferrin and albumin proteins, which transport and solubilise iron within cytoplasm and thereby exploiting the body's inherent mechanism for the safe and non-toxic delivery of iron.[13,14]

Within the "ruthenotherapy",[15–19] the sodium salt analogue NKP-1339 has progressed into clinical trials.[20] Also, the ruthenium(II)-arene 1,3,5-triaza-7-phosphaadamantane (RAPTA) compound, exhibits substantial cytotoxicity against a number of cancer lines and induces cell death primarily *via* mitochondrial apoptosis.[21,22] Moreover, both RM175 and ONCO4417 induce apoptosis through G2/M phase arrest. Noticeably, ONCO4417 also exhibits DNA-damaging properties at levels similar to cisplatin.[23]

Another class of ruthenium(II) based complexes which have gained significant interest in the development of anticancer agents are those supported on arene scaffolds.[24–28] This is

---

[a] *School of Chemistry and Physics, University of KwaZulu-Natal, Private Bag X01, Scottsville, Pietermaritzburg 3209, South Africa. E-mail: ojwach@ukzn.ac.za*

[b] *Department of Science and Innovation/Mintek Nanotechnology Innovation Centre, Biolabels Research Node, Department of Biotechnology, University of the Western Cape, Bag X17, Bellville, 7535, Cape Town, South Africa*

† Electronic supplementary information (ESI) available: Experimental methodologies and analytical findings, which encompass NMR and FT-IR spectroscopic spectra, mass spectrometry data, X-ray crystallography data, and associated files. Additionally, it includes electronic and emission curves for DNA and protein interactions, *in silico* molecular docking diagrams, and various biological graphs. The crystallographic data entry for **Ru2** is made available through the deposition number. CCDC 2304942. For ESI and crystallographic data in CIF or other electronic format see DOI: https://doi.org/10.1039/d4ra00525b

‡ Current address: Department of Chemistry, University of Cape Town, Rondebosch, 7701, South Africa.

attributed to their distinct characteristics, including solubility, stability, lipophilicity, and accessibility *via* facile synthetic routes. One such example, is the investigations of the *in vitro* cytotoxicity of ruthenium(II)–arene complexes of N-heterocyclic carbene (NHC) ligands.[29,30] These complexes exhibit good lipophilicity and show high accumulation within the A2780 cell line. It has also been observed that Ru(II)–arene complexes containing perfluorinated phosphine ligands, show improved cytotoxicity and selectivity.[31,32] In another related study involving the assessment of antiproliferative activity and apoptosis mechanism of arene Ru(II) carbazole-based hydrazone complexes, it was found that the complexes display comparable cytotoxicity to cisplatin.[33]

To broaden the spectrum and chemical diversity of the currently available Ru(II) based anticancer drugs, we report the synthesis and structural studies of novel Ru(II) complexes functionalized on the (pyrazine)carboxamide scaffolds. The interactions of these complexes with DNA and protein were also explored using spectroscopic and molecular docking techniques. The cytotoxic effects of the complexes on a panel of six cell lines were also evaluated and are herein discussed.

Results and discussion

Synthesis and structural characterisation of the ruthenium(II) complexes

The carboxamide ligands *N*-(^{1}H-benzo[*d*]imidazol-2-yl)pyrazine-2-carboxamide (**HL$_1$**), and *N*-(benzo[*d*]thiazol-2-yl)pyrazine-2-carboxamide (**HL$_2$**) were synthesized by following established literature procedures[34,35] and were obtained in moderate to good yields of 52% (**HL$_1$**) and 85% (**HL$_2$**) as depicted in Scheme 1. Reactions of ligands **HL$_1$** and **HL$_2$** with [RuCl$_2$(*p*-cymene)]$_2$ in the presence of NaOMe in a 1 : 2 mole ratio in absolute ethanol afforded complexes [Ru(L$_1$)(*p*-cymene)Cl] (**Ru1**) and [Ru(L$_2$)(*p*-cymene)Cl] (**Ru2**) in high yields of 72% and 84% respectively (Scheme 1). Similarly, reactions of equimolar amounts of ligands **HL$_1$** and **HL$_2$** with RuCl$_2$(PPh$_3$)$_3$ in CH$_2$Cl$_2$ afforded the respective complexes [Ru(L$_1$)(PPh$_3$)$_2$Cl] (**Ru3**) and [Ru(L$_2$)(PPh$_3$)$_2$Cl] in moderate and low yields of 66% and 47% respectively (Scheme 1).

Structural identities of ligands (**HL$_1$** and **HL$_2$**) and their corresponding complexes **Ru1–Ru4** were confirmed by a combination of ^{1}H, ^{13}C, ^{31}P NMR, FT-IR spectroscopies, mass spectrometry, elemental analysis, and single crystal X-ray analysis (**Ru2**). For example, in the ^{1}H NMR spectrum of **HL$_1$** (Fig. S1†), distinctive singlet at 12.20 ppm was observed, corresponding to two protons of the N–H from the benzimidazole and from the sec amide. Upon the formation of **Ru1** (Fig. S3†) one signal disappeared, serving as clear evidence of the deprotonation of the N–H amide group during the metalation process. Similar observations were made in the ^{1}H NMR spectra of complexes **Ru2–Ru4** (Fig. S4–S6†). Furthermore, to confirm the identities of **Ru3** and **Ru4**, we employed ^{31}P NMR and sharp singlets were observed at 26.10 ppm for **Ru3** and 26.47 ppm for **Ru4** (Fig. S7 and S8†). These resonances are consistent with the presence of two magnetically equivalent PPh$_3$ groups arranged in *trans* configuration, consistent with the proposed structures in Scheme 1.[36,37] In addition, the formation and identity of complexes **Ru1–Ru4**, was also derived from comparisons of their ^{13}C NMR spectral data to those of their respective ligands (Fig. S9–S13†). For instance, the carbonyl resonance peak at 161.6 ppm (**HL$_1$**) is slightly shifted to 167.9 ppm in the corresponding complex **Ru1** (Fig. S9 and S11†).

The chemical identities of compounds **Ru1–Ru4** were additionally ascertained from their FT-IR spectra (Fig. S14–S19†). As an illustration, the C═O stretching band at 1691 cm^{-1} in **HL$_1$** (Fig. S14†) is shifted downfield to 1625 cm^{-1} in **Ru1** (Fig. S16†). This observation is likely due to π-back donation, from the d-orbitals of the Ru(II) to the unoccupied π* orbitals of the ligands. Noteworthy, the C═O signals remained within the expected range for C═O signal, indicating no keto–enol tautomerization, contradicting earlier reports by Gupta and their colleagues.[38]

Mass spectrometry was also utilized to elucidate the molecular composition of the isolated complexes (Fig. S20–S25†). The positive ion ESI-MS spectra show the base peaks at $m/z = 510.05$ (calcd 509.06, 100%) for **Ru1**, 527.03 (calcd 526.02, 100%) for **Ru2**, 899.13 (calcd 900.14) for **Ru3**, corresponding to the protonated molecular ion [M+H]$^+$ ions. The positive HR-MS spectra of **Ru4** showed a signal at $m/z = 917.0967$ (100%) and thus deviating from the calculated mass (917.0974) with an acceptable difference of 0.0007. Elemental analyses data of complexes **Ru1–Ru4** were consistent with the empirical formulae of the proposed structures in Scheme 1 and proved their purity in bulk state.

Molecular structure of complex Ru2

Single crystals suitable for X-ray analysis of complex **Ru2** were grown by slow diffusion of diethyl ether into a concentrated solution of ethanol at room temperature. Fig. 1 depicts the

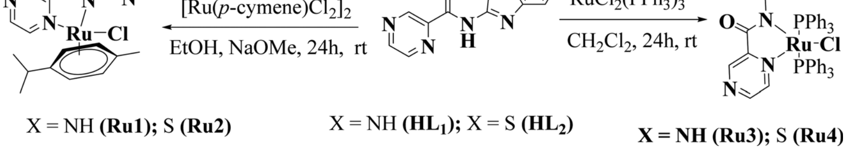

Scheme 1 Synthetic route of ligands and the corresponding Ru(II) complexes.

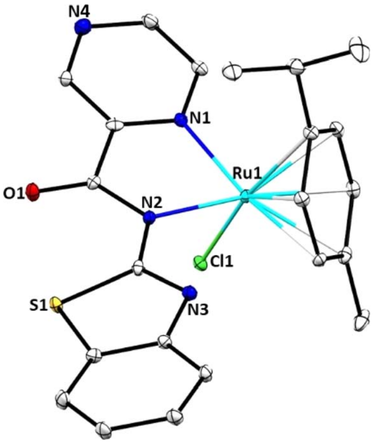

Fig. 1 Molecular structure diagram of **Ru2** showing atom numbering scheme Selected bond lengths (Å) and angles (°): Ru(1)–N(1), 2.098(7); Ru(1)–N(2), 2.131(7); Ru(1)–Cl(1), 2.404(2); Ru(1)–C(18), 2.209(9); Ru(1)–C(20), 2.189(8), Ru(1)–C(17), 2.169(8), Ru(1)–C(16), 2.217(9), Ru(1)–C(21), 2.187(8); Ru1–C19, 2.238. N(1)–Ru(1)–N(2), 77.5(3); N(1)–Ru(1)–Cl(1), 83.0(2), N(2)–Ru(1)–Cl(1), 82.31(19), N(1)–Ru(1)–C(18), 102.8(3); N(1)–Ru(1)–C(20), 169.5(3); N(1)–Ru(1)–C(17), 91.6(3); N(1)–Ru(1)–C(16), 108.0(3); N(1)–Ru(1)–C(21), 142.6(3).

molecular structure of **Ru2**, with thermal ellipsoids at 50%, while Table S1† contains crystallographic data and structure refinement parameters. The complex crystallizes in the monoclinic system with C2 space group. In the molecular structure of **Ru2**, the Ru(II) atom contains one mono-anionic bidentate bound ligand ($\mathbf{L}^{-}{}_{2}$) and adopts a three-legged piano-stool arrangement. The coordination sphere around the Ru(II) atom in **Ru2** is formed by the π-bonded *p*-cymene ring situated at the apex, while the N(1) and N(2) donor atoms of the bidentate ligand $\mathbf{L_2}$, along with the chlorido ligand, are conformationally located on the base of the piano stool-like structure. This arrangement forms a five-membered chelate ring with the Ru(II) ion. The dihedral angles for N(1)–Ru(1)–Cl(1) of 83.0(2)° and N(2)–Ru(1)–Cl(1), 82.31(19)° significantly depart from the expected 90°. Additionally, the bite angle for N(1)–Ru(1)–C(20), of 169.5(3)° deviates appreciably from linearity of 180°. Consequently, the geometry around the Ru(II) centre can best be described as distorted octahedral configuration. The N(1) and N(2) atoms are coordinated to the Ru(II) ion with almost equal bond distances (Ru(1)–N(1), 2.098(7); Ru(1)–N(2), 2.131(7)), signalling the absence of keto–enol tautomerization as observed in the spectral data. The bond length Ru(1)–N(1), 2.098(7) Å falls within the average value of 2.089 ± 0.014 Å reported for 18 related structures.[39] The bond length Ru(1)–Cl(1), 2.404(2) Å correlate well with the mean distance of 2.411 ± 0.014 Å obtained for 33 similar structures.[40]

Solution stability of complexes Ru1–Ru4

The solution stability of complexes **Ru1–Ru4** was evaluated in both aqueous and DMSO media using UV-vis and ^{1}H NMR spectroscopies, respectively. Fig. S26 and S28† show representative time-dependent UV-vis spectral scans of **Ru4** and **Ru2**, respectively in PBS. The complexes showed characteristic peaks at 260 nm and their profiles remained largely invariant over the 72 h period. This implies that no structural changes occurred, hence stability of the complexes under the physiological conditions used in the DNA interactions and *in vitro* studies. Typical ^{1}H NMR spectra of complexes **Ru1** and **Ru2** in DMSO-d_6 are shown in Fig. S28 and S29,† respectively. Consistent with the UV-visible data, there were no noticeable changes in proton chemical shifts, suggesting the stability of the complexes in DMSO over the 48 h period.

DNA binding studies

Absorption spectroscopic measurements. Platinum group metals primarily exert their mode of action by binding to the DNA molecule, thereby impeding the synthesis and replication processes.[41–43] This interference ultimately leads to cell death.[44] DNA titration experiments help in understanding how molecules interact with DNA, which is crucial in various biological processes such as gene regulation, DNA replication, and repair. We thus used electronic absorption spectroscopy to examine the strength and mode of interactions between complexes **Ru1–Ru4** and CT-DNA under varying concentrations of CT-DNA (Fig. 2 and S30–S33†). The prominent absorption band at ∼270 nm is attributed to intra-ligand π → π* charge transfer transitions. Notably, hyperchromic shift in absorbance is observed for **Ru1** and **Ru2**, resulting from the secondary damage of CT-DNA double helix. This observation indicates that the interactions of the complexes with CT-DNA are primarily either *via* an electrostatic, major, or minor groove modes.[45] In contrast, the absorption bands for **Ru3** and **Ru4** depict a considerable reduction in absorbance (hypochromic shift), which can be ascribed to the conformational changes in the DNA helical structure. To enable a quantitative comparison of CT-DNA binding affinities, the intrinsic binding constant (K_b) and Gibb's free energies (ΔG) were calculated from the spectral data using eqn S1 and S2† respectively.

The K_b values for complexes **Ru1–Ru4** fall within the range of 0.21–9.22 × 10^6 M^{-1} (Table 1). Strikingly, complexes **Ru1** and **Ru3**, which contain the NH moiety, exhibited higher K_b values in comparison to the benzothiazole analogues **Ru2** and **Ru4.** We have previously reported similar trends using related Pd(II)

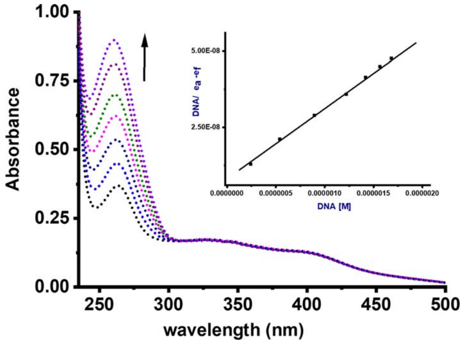

Fig. 2 Electronic absorption spectrum of complex **Ru2** in the presence of increasing concentration of CT-DNA in PBS buffer. (Inset) Plot of [CT-DNA] *vs.* [DNA]/($\varepsilon_a - \varepsilon_f$). The arrow depicts hyperchromic shift on the addition of increasing quantities of DNA.

Table 1 CT-DNA-binding constants derived from the UV-vis and EB-DNA fluorescence experiments

	UV-vis titration		EB fluorescence emission titration				
Compound	K_b 10^6 M^{-1}	$\Delta G^{\ddagger}_{25°C}$/kJ mol^{-1}	K_{sv} 10^4 M^{-1}	K_q 10^{11} M^{-1}	K_{app} 10^6 M^{-1}	K_F 10^2 M^{-1}	n
Ru1	9.22 ± 0.75	39.73	1.01 ± 0.28	1.01 ± 0.29	2.96 ± 0.23	1.30 ± 0.10	0.99
Ru2	0.32 ± 0.01	31.40	0.51 ± 0.07	0.51 ± 0.01	2.44 ± 0.12	0.51 ± 0.06	0.95
Ru3	3.92 ± 0.46	37.61	1.84 ± 0.21	1.84 ± 0.11	3.41 ± 0.28	2.24 ± 0.16	0.99
Ru4	0.21 ± 0.01	30.36	1.65 ± 0.22	1.65 ± 0.63	3.01 ± 0.28	1.13 ± 0.10	0.97

complexes.[7] A plausible explanation for this phenomenon could be due to the hydrogen bonding interactions between the NH group of carboxamide and DNA nucleobases, thereby enhancing the strength and extent of these interactions. It is important to note that the K_b values for compounds **Ru1** and **Ru2**, were higher than those of related Ru(II) cymene with (poly) cyclic aromatic diamine ligands (0.4–1.0 × 10^4).[46] The negative ΔG values for compounds **Ru1–Ru4** signify spontaneous interactions with CT-DNA.[47]

Ethidium competitive assay

To confirm the interactions between compounds **Ru1–Ru4** and CT-DNA, a fluorescent-quenching assay using EtBr dye was conducted at varying concentrations of metal complexes (Fig. S34–S37†). Interestingly, there was an approximate 18% reduction (hypochromic shift) observed at 600 nm, alluding to the limited ability of compounds **Ru1–Ru4** to displace EtBr from the EtBr-CT-DNA adduct and effectively intercalate with the CT-DNA base pairs.[48] The Stern–Volmer quenching constant (K_{sv}), bimolecular quenching rate constant (k_q) and apparent binding affinity constants (K_{app}) were derived from the Stern–Volmer equations eqn S3 and S4† (Table 1). Additionally, the Scatchard equation, eqn S5 was employed to calculate the association binding constant (K_F) and the number of binding sites per nucleotide (n) as summarized in Table 1. The K_{sv} values for compounds **Ru1–Ru4** ranged from 0.51 to 1.84 × 10^4 M^{-1}. Noticeably, the values of K_{sv} are 10^3 to 10^4 fold lower than that of the classical intercalator EtBr (10^7 M^{-1}),[49] further hinting on the weaker interactions of compounds **Ru1–Ru4** with CT-DNA in comparison EtBr. The obtained k_q values, with a magnitude of 10^{11} M^{-1} are ten times higher than the upper limit (2.0 × 10^{10} L mol^{-1} s^{-1}) observed for quenching rate constants in dynamic interactions.[50] This substantial difference strongly suggests the existence of static quenching mechanism. Similarly, the magnitude of K_{app} (10^6 M^{-1}) is lower compared to the binding constants typically associated with the classical intercalators (10^7 M^{-1}),[51] further underscoring the existence of weak intercalative interaction. The K_F values (10^1–10^2 M^{-1} magnitude) also indicate that the complexes have weak quenching efficiencies. The values of $n \approx 1$, imply the presence of one binding site for every two base pairs.

Hoechst 33258 displacement assay

To further elucidate the precise mechanism of interaction between these complexes and CT-DNA, we performed competitive binding assay involving Hoechst 33258 dye. The characteristic emission curves of Hoechst-CT-DNA, in the presence of varying quantities of Ru(II) complexes are depicted in Fig. 3 (**Ru2**) and ESI Fig. S38–S41† for the other complexes. The intensity of the emissions at 450 nm decreases significantly by *ca.* 45% upon addition of increasing amounts of compounds **Ru1–Ru4**. This observation strongly confirm that the complexes participate in competitive binding with Hoechst 33258 and simultaneously interact with the minor groove of CT-DNA.[52]

The values of the binding constants of K_{sv}, K_q, K_{app} and K_F with the Hoechst 33258 dye are presented in Table 2. These values are higher compared to those observed for EtBr displacement, signalling that compounds **Ru1–Ru4** prefer a stronger and more favourable binding interaction through the minor groove of the CT-DNA rather than *via* an intercalative mode. The K_{sv} values ranged from 1.71 to 7.90 × 10^5 M^{-1} and are consistent with the affinity observed in other Ru(II) complexes known for groove binding mode.[53] The magnitude of the k_q value of 10^{12} M^{-1} considerably exceeds the collision quenching constant of biomolecules (2.0 × 10^{10} L mol^{-1} s^{-1}), indicating the presence of static mode of quenching.[54] We note that the K_{app} values (magnitude 10^6–10^7 M^{-1}) of compounds **Ru1–Ru4** are greater than those of analogous compounds abound in literature, which fall within the range of 10^4–10^5 M^{-1}.[55] Both EtBr and Hoesch displacement studies reveal a dual mode of interactions between **Ru1–Ru4** and CT-DNA, entailing partial intercalation and strong minor groove interactions.

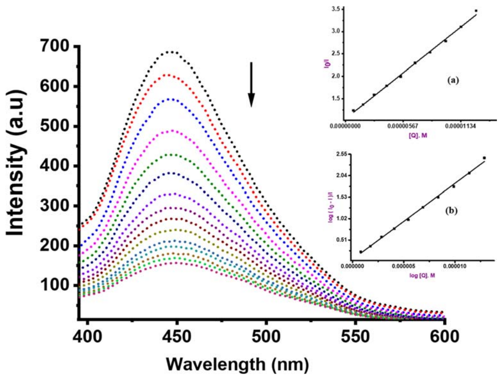

Fig. 3 Emission of Hoechst 33258 for **Ru2**: [H258] = 15 μM and [**Ru2**] = 0–22 μM. The arrow shows the intensity changes upon increasing the concentration of **Ru2**. (Insets) (a) Stern–Volmer plot of I_0/I *vs.* [Q] and (b) Scatchard plot of log[(I_0−I)/I] *vs.* log[Q].

Table 2 Quenching constants obtained from Hoe-CT-DNA fluorescence assay

	Hoechst 33258 displacement			
Compound	K_{sv} 10^5 M^{-1}	K_q 10^{12} M^{-1}	K_{app} 10^7 M^{-1}	K_F 10^4 M^{-1}
Ru1	7.90 ± 0.29	7.90 ± 0.66	2.27 ± 0.15	0.64 ± 0.07
Ru2	1.71 ± 0.01	1.71 ± 0.14	0.44 ± 0.02	0.12 ± 0.01
Ru3	9.74 ± 0.25	9.74 ± 0.76	1.44 ± 0.17	6.1 ± 0.55
Ru4	1.82 ± 0.01	1.82 ± 0.14	0.51 ± 0.06	4.33 ± 0.39

Table 3 BSA binding constants, and number of binding sites

	Fluorescence titration			
Compound	K_{sv} 10^4 M^{-1}	K_q 10^{11} M^{-1}	K_F 10^2 M^{-1}	n
Ru1	4.01 ± 0.24	4.01 ± 0.28	2.61 ± 0.19	0.83
Ru2	0.72 ± 0.05	0.72 ± 0.15	0.13 ± 0.01	0.71
Ru3	1.96 ± 0.13	1.96 ± 0.38	1.01 ± 0.10	0.93
Ru4	1.43 ± 0.13	1.43 ± 0.37	1.42 ± 0.11	0.85

Protein interactions

Serum albumin primarily functions as a carrier for a wide range of molecules, including drugs, within the bloodstream and thus ensuring the delivery of the pharmaceuticals to their intended targets within the body.[56] Our choice of the bovine serum albumin (BSA) as a model protein was driven by its structural similarity, sharing approximately 76% homology to the human serum albumin (HSA).[56,57] The emission as a result of the presence of tryptophan (Trp) amino acid residues, specifically Trp-212 and Trp-134 located within the subdomains IIA and 1B, respectively was observed and recorded at 350 nm.[58,59] The spectra were recorded over a range spanning from 300 to 420 nm, while varying the concentration of the metal complexes (Fig. S42–S45†). A considerable reduction in the fluorescence intensity was observed (Fig. 4) and attributed to binding with Trp-134 and Trp-213 residues situated within the hydrophobic cavity.[60,61]

The values for K_{sv}, k_q, K_F and n are presented in Table 3. The K_{sv} values, ranging from 0.72 to 4.01 × 10^4 M^{-1}, are approximately three to four orders of magnitude lower than those observed for classical intercalators, falling in the range of 10^7 M^{-1}.[62] The lower K_{sv} values show that the interaction between the complexes and BSA is not fully controlled by diffusion. This is augmented by the higher k_q values, with magnitude of 10^{11} M^{-1} s^{-1}, which surpasses those of known associative biopolymers (2.0 × 10^{10} M^{-1} s^{-1}), and points to the involvement of static quenching mechanism.[63,64] The K_F values, with a magnitude of 10^1–10^2 M are significantly lower than the association constant of 10^{15} M^{-1} for irreversible interactions. This disparity suggests that the complexes bind reversibly to BSA.[65,66] The n values are close to 1, indicating that each complex has only one binding site in the BSA.

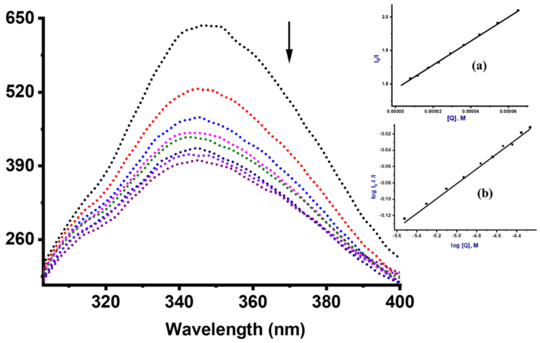

Fig. 4 Emission spectrum of BSA in the presence of consecutive quantities of complex Ru2, PBS buffer at room temperature. The arrow shows the intensity changes upon increasing Ru2 concentration. (Insets) (a) Stern–Volmer plot of I_0/I *vs.* [Q] and (b) Scatchard plot of log [(I_0−I)/I] *vs.* log[Q].

Molecular docking

Molecular docking techniques was used to predict the preferred orientation of the molecules when bound to the receptor to form stable complexes. The approach is used to further substantiate the observed experimental binding constants, mode of interactions and location of binding in the biomolecules. Specifically, we conducted simulations of compounds **Ru1–Ru4** within the DNA dodecamer and BSA protein. Distinctively, the docked poses of **Ru1–Ru4** demonstrate binding to the nucleotide residues within the minor groove of DNA double helix (Fig. 5), in tandem with the experimental results. Conventional hydrogen bond interactions participate with DG22 (**Ru1**, 2.85 Å), and DA5 (**Ru4**, 3.08 Å). The stability of compound **Ru1** is also contributed by the favourable-acceptor–acceptor interaction formed with DC3 (2.94 Å). Similarly, carbon hydrogen bond interactions (with DC23, 3.46 Å) stabilize **Ru2** in the groove. Nucleotides DG4 (for **Ru3**, 5.18 Å and **Ru4**, 5.11 Å) and DA17 (for **Ru3**, 5.45 Å) are involved in pi–alkyl interactions. Additionally, **Ru3** is surrounded by DA18 (1.80 Å) *via* unfavourable donor–donor interaction. The binding scores of −8.2 kcal mol^{-1} (**Ru1**), −8.0 kcal mol^{-1} (**Ru2**), −7.7 kcal mol^{-1} (**Ru3**), and −7.4 kcal mol^{-1} (**Ru4**), show a rough positive correlation with the spectroscopic binding constants as provided in Tables 2 and 3

The interactions of compounds **Ru1–Ru4** with BSA receptor are depicted in Fig. 6. The poses of the complexes are predominantly surrounded by the hydrophobic amino acid residues, characterized by hydrophobicity values ranging from −3.00 to 3.00 (Fig. S46 and S47† for **Ru1** and **Ru2**, respectively). Alkyl interactions dominate compound **Ru1** (with ILE522, 5.05 Å; VAL423, 4.98 Å; PRO420, 5.09 Å), **Ru2** (ILE522, 5.02 Å; VAL423, 5.06 Å), **Ru3** (CYS447, 4.90 Å; TYR451, 5.34 Å; LYS294, 4.44 Å) and **Ru4** (ILE522, 4.75 Å; PRO420, 4.96 Å; LYS114, 4.73 Å active residues). Conventional hydrogen bonding interactions are observed in **Ru1** (ARG458, 2.47 Å), **Ru2** (GLU424, 2.13 Å; HIS145, 3.44 Å; ARG144, 2.71 Å) and **Ru4** (LEU112, 2.51 Å). Furthermore, **Ru1** interacts associatively with ASP108 (3.78 Å) through carbon hydrogen interaction. Moreover, **Ru4** is confined in the neighbourhood of LEU112 (3.10 Å) *via* sulfur interactions. The docking scores of −8.0, −7.6, −6.6–6.3 kcal mol^{-1} for **Ru1**, **Ru2**, **Ru3** and **Ru4** (Fig. 5), nearly match the trend for experimental values, shown in Table 3.

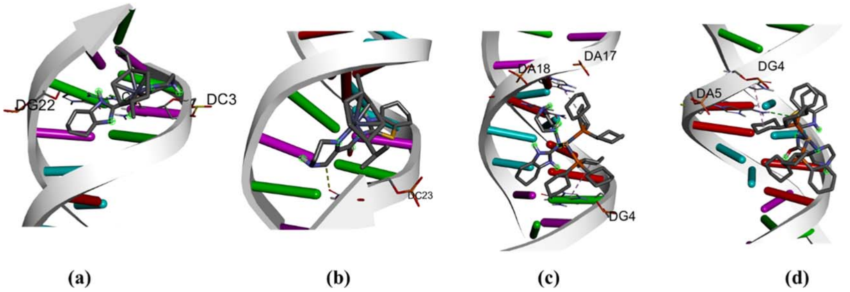

Fig. 5 Top ranked DNA surface pocket pose of (a) **Ru1**, (b) **Ru2**, (c) **Ru3**, and (d) **Ru4** represented as stick diagrams, displaying minor groove binding. The DNA binding affinities of **Ru1**, **Ru2**, **Ru3**, and **Ru4** are distinguished by their respective binding scores, which measure −8.2, −8.0, −7.7, and −7.4 kcal mol^{-1}.

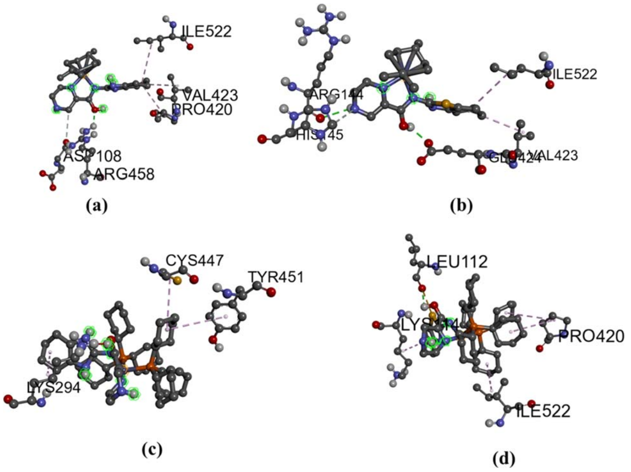

Fig. 6 BSA interactions diagram (scaled ball and stick), (a) **Ru1** (b) **Ru2** (c) **Ru3** and **Ru4** (d), with binding scores of −8.0 (**Ru1**), −7.6 kcal mol^{-1} (**Ru2**), 6.6 kcal mol^{-1} (**Ru3**) and −6.3 kcal mol^{-1} (**Ru4**).

In vitro cytotoxicity

The cytotoxic effects of **Ru1–Ru4** complexes were assessed against six human cell lines; lung cancer (A549), prostate cancer (PC-3), colon cancer (HT-29 and Caco-2), Caco-2 (colon cancer), cervical cancer (HeLa) and normal skin fibroblast (KMST-6) cells. Cell viability was quantified by MTT assay following 24 h treatment. Since DMSO was used as the solvent for the complexes at 0.1%, it was also incorporated as a vehicle control. Percentage cell survival studies clearly indicated that **Ru1–Ru4** complexes exhibited a dose-dependent cytotoxic activity (Fig. S48†). Cytotoxicity of these complexes increased proportionally as their concentration increased from 6.25 to 100 μg mL^{-1}. The resultant IC_{50} values were calculated using dose–response curve fitting analysis, and the values were subsequently compared with those of cisplatin (Table 4). Significantly, **Ru1** and **Ru2** complexes displayed remarkable potency, surpassing the efficacy of cisplatin in certain cases, especially against A549, PC-3, HT-29, and Caco-2 cells (for **Ru1**) cell (Table 4). Moreover, both **Ru1** and **Ru2** exhibited SI > greater than 2, indicating their selectivity towards the cancer cells over the normal cells.

Evidently, the introduction of *p*-cymene appears to enhance the biological activity of the complexes. In HeLa cells for example, the *p*-cymene **Ru1** complex showed lower percentage cell viability and IC_{50} of 5.47 μg mL^{-1} compared to the value of >100 μg mL^{-1} displayed by the corresponding PPh_3 **Ru3** complex (Table 4). These results mirrored the previous findings and has been associated with the improved stability of the arene complexes, in addition to improved lipophilic properties.[66,67] In the case of **Ru3** and **Ru4** complexes, bearing the PPh_3 co-ligands, their poor cytotoxicity could also be attributed to the steric crowding effect of the bulky PPh_3 group, which ultimately limited the interaction of the complexes with the DNA and BSA protein. However, this explanation contradicts their derived spectroscopic constants, which depict higher values compared to their counterparts **Ru1** and **Ru2**. In addition to the poor cytotoxicity of **Ru3** and **Ru4**, their poor selectivity (SI ≤ 1) imply that these PPh_3 complexes are not good candidates for cancer treatment.

Table 4 Cytotoxic potencies and cancer-cell selectivity of **Ru1–Ru4** complexes[a]

	IC_{50} (μM)						Selective index (SI)				
Compound	KMST-6	A549	PC-3	HT-29	Caco-2	HeLa	A549	PC-3	HT-29	Caco-2	HeLa
Ru1	20.31 ± 2.68	3.29 ± 1.01	0.08 ± 0.03	7.54 ± 2.87	5.38 ± 0.02	5.47 ± 0.58	>2	>2	>2	>2	>2
Ru2	>100	2.38 ± 0.20	6.26 ± 1.41	21.84 ± 3.47	17.16 ± 1.53	31.09 ± 4.81	>2	>2	>2	>2	>2
Ru3	6.78 ± 0.19	>100	>100	>100	>100	>100	0.06	0.06	0.06	0.06	0.06
Ru4	>100	22.88 ± 0.15	>100	>100	>100	>100	>2	1	1	1	1
Cisplatin	38.8 ± 13.29	91.8 ± 5.89	9.2 ± 1.73	17.4 ± 4.54	18.16 ± 0.86	3.76 ± 0.93	0.51	>2	>2	>2	>2

[a] >100 denotes that IC_{50} was undetermined at the test concentrations (0–100 μM).

Conclusions

In summary, the present stud describes in detail the synthesis and structural characterization of heterocyclic (pyrazine)carboxamide Ru(II) complexes. The spectroscopic methods indicate that the complexes are sufficiently stable in aqueous and physiological conditions. The interactions between the Ru(II) complexes (**Ru1**–**Ru4**) and CT-DNA reveal two distinct binding modes, namely minor groove binding and partial intercalation. When interacting with BSA protein, both experimental and molecular docking results show that the complexes exhibit favourable non-covalent interactions with the Trp residues within the hydrophobic cavity. The *p*-cymene complexes **Ru1** and **Ru2** demonstrated higher cytotoxic efficacy than the PPh_3 counterparts **Ru3** and **Ru4**. More significantly, the cytotoxicity and selectivity of complexes **Ru1** and **Ru2** against A549, PC-3, and Caco-2 cell lines surpassed that of cisplatin.

Experimental section

Synthesis of Ru(II) complexes

Synthesis of [Ru(*N*-(^{1}H-benzo[*d*]imidazol-2-yl)pyrazine-2-carboxamide)Cl] (Ru1). To a solution of dichloro(*p*-cymene) ruthenium(II) dimer (0.05 g, 0.08 mmol) in absolute ethanol, *N*-(^{1}H-benzo[*d*]imidazol-2-yl)pyrazine-2-carboxamide (**L1**) (0.01 g, 0.04 mmol) and NaMeO (0.01 g, 0.18 mmol) were added, and the suspension stirred at room temperature for 4 h. The resulting solution was filtered over Celite, the filtrate was concentrated, and diethyl ether (40 mL) was added. The precipitate was filtered and dried in a vacuum to afford desired product (**Ru1**) as an orange solid. Yield: 0.015 g (72%). ^{1}H NMR (400 MHz, DMSO) δ 13.12 (s, $1H_{N\text{–}H}$) 9.54 (dd, $^3J_{HH}$ = 4.2, 1.1 Hz, $1H_{pyz}$), 9.27 (d, $^3J_{HH}$ = 1.0 Hz, $1H_{pyz}$), 9.12 (d, $^3J_{HH}$ = 3.0 Hz, $1H_{bz}$), 7.75 (dd, $^3J_{HH}$ = 3.2 Hz, $2H_{bz}$), 7.45 (dd, $^3J_{HH}$ = 3.0, 2.7 Hz, $2H_{bz}$), 6.20 (d, $^3J_{HH}$ = 6.0 Hz, 1H, cymene *CH*), 6.09 (d, $^3J_{HH}$ = 6.0 Hz, 1H, cymene *CH*), 6.04 (d, $^3J_{HH}$ = 6.0 Hz, 1H, cymene *CH*), 5.95 (d, J_{HH} = 6.0 Hz, 1H, cymene CH_2), 2.63 (sept, $^3J_{HH}$ = 7.2 Hz, 1H, $CHMe_2$), 2.24 (s, 3H, *Me*), 1.11 (d, 3H, $CHMe_2$), 1.01 (d, 3H, $CHMe_2$), ^{13}C NMR (400 MHz, DMSO-d_6): δ 18.80, 22.13, 30.95, 58.08, 63.09, 72.05, 72.12, 113.91, 122.87, 147.28, 150.25, 167.90. FT-IR spectrum (Zn–Se ATR, cm^{-1}): 1625 (C=O), 1542 (C=N). TOF MS-ES, *m*/*z* (%) 509.0454. Found 510.0543 (M^++H). Anal calcd (%) for $C_{22}H_{22}N_5ClRuO$: C, 51.39; N, 9.85; H, 3.95% found: C, 51.62; N, 9.76; H, 3.60%.

Synthesis of [Ru(*N*-(benzo[*d*]thiazol-2-yl)pyrazine-2-carboxamide)Cl] (Ru2). Complex **Ru2** was prepared following the procedure described for **Ru1** using *N*-(benzo[*d*]thiazol-2-yl) pyrazine-2-carboxamide (**L2** (0.01 g, 0.04 mmol) and dichloro(*p*-cymene)ruthenium(II) dimer (0.05 g, 0.08 mmol). Orange solid. Yield: 0.018 g (84%). ^{1}H NMR (400 MHz, d_6-DMSO): 9.53 (d, $1H_{pyz}$), 9.18 (s, $^3J_{HH}$ = 2.4 Hz, $1H_{pyz}$), 8.99 (d, $1H_{pyz}$), 7.90 (dd, $^3J_{HH}$ = 7.8 Hz, $2H_{pyz}$), 7.45 (dd, $^3J_{HH}$ = 8.0 Hz, $1H_{bz}$), 7.30 (d, $^3J_{HH}$ = 7.6 Hz, $1H_{bz}$), 5.81(d, $^3J_{HH}$ = 6.0 Hz, 2H, cymene *CH*), 5.76 (d, $^3J_{HH}$ = 6.0 Hz, 2H, cymene *CH*), 2.84 (sept, $^3J_{HH}$ = 7.2 Hz, 1H, $CHMe_2$), 2.09 (s, 3H, *Me*), 1.21 (d, 6H, $CHMe_2$), ^{13}C NMR (400 MHz, DMSO-d_6): δ 19.17, 21.76, 30.99, 121.24, 121.55, 125.90, 133.73, 146.94, 147.71, 149.52, 165.58, 168.39. FT-IR spectrum (Zn–Se ATR, cm^{-1}): 1626 (C=O), 1586 (C=N). TOF MS-ES, *m*/*z* (%) 526.0245; found 527.0325 (M^++H). Anal calcd (%) for $C_{22}H_{21}N_4ClRuOS$: C, 50.04; N, 10.17; H, 3.86% found: C, 50.23; N, 10.65; H, 4.02%.

Synthesis of [*N*-(1*H*-benzo[*d*]imidazol-2-yl)pyrazine-2-carboxamide $RuCl_2(PPh_3)_2$] (Ru3). To a solution of ligand **L1** (0.01 g, 0.05 mmol) in CH_2Cl_2 (5 mL) was added to a solution of $RuCl_2(PPh_3)_3$ (0.05 g, 0.05 mmol) in CH_2Cl_2 (5 mL) to give a light brown precipitate. The mixture was stirred for 4 h at room temperature and filtered to obtain a dark brown precipitate. Recrystallization of the crude product in CH_2Cl_2 afforded compound **Ru3** as analytically pure brown solid. Yield: 0.03 g (66%). ^{1}H NMR (400 MHz, d_6-DMSO): δ 6.90(t, $^3J_{HH}$ = 7.0 Hz, PPh_3, 3H), 7.05(t, $^3J_{HH}$ = 9.0 Hz, 2H), 7.16(m, PPh_3, 7H); 7.23(m, PPh_3, 5H), 7.41(m, PPh_3, 11H), 7.50(dd, $^3J_{HH}$ = 6.0 Hz, 2H), 7.64(m, PPh_3, 4H), 8.82(d, $^3J_{HH}$ = 4.0 Hz, 1H), 8.90(d, $^3J_{HH}$ = 2.1 Hz. 1H), 9.36(d, $^3J_{HH}$ = 1.4 Hz, 1H), ^{13}C NMR (400 MHz, DMSO-d_6): δ 123.05, 128.07, 128.08, 136.02, 136.60, 137.04, 138.07, 141.05, 144.07, 145.00, 162.45. ^{31}P{^{1}H} NMR (d_6-DMSO, δ): 26.10, FT-IR spectrum (Zn–Se ATR, cm^{-1}): 1617 (C=O), 1566 (C=N). TOF MS-ES, *m*/*z* (%) 899.1335; found 900.1415 (M^++H) anal calcd (%) for $C_{48}H_{38}N_5ClOP_2Ru$: C, 58.87; N, 7.01; H, 3.86; found: C, 58.71; N, 7.39; H, 4.06%.

Synthesis of [(*N*-(benzo[*d*]thiazol-2-yl)pyrazine-2-carboxamide) $RuCl_2(PPh_3)_2$] (Ru4). The procedure described for **Ru3** was followed for the synthesis of **Ru4**, using ligand **L2** (0.013 g, 0.05 mmol) and $RuCl_2(PPh_3)_3$ (0.05 g, 0.05 mmol) brown solid. Recrystallization of the crude product in CH_2Cl_2 afforded compound **Ru4** as analytically pure brown solid yield: 0.025 g (47%). ^{1}H NMR (400 MHz, d_6-DMSO): δ 7.23(m, PPh_3, 2H), 7.35(m, PPh_3, 4H), 7.40(m, PPh_3, 10H); 7.53(m, PPh_3, 15H), 7.55(d, 1H), 7.59(d, $^3J_{HH}$ = 11.46 Hz, 2H), 8.85(dd, $^3J_{HH}$ = 11.04 Hz, 1H), 8.95(d, $^3J_{HH}$ = 3.2 Hz, 1H), 9.93(d, $^3J_{HH}$ = 1.46 Hz. 1H), ^{13}C NMR (400 MHz, DMSO-d_6): δ 122.35, 124.53, 125.76, 126.83, 127.73, 127.81, 129.90, 132.72, 133.78, 134.26, 137.12, 144.97, 148.87, 168.06, 177.09. ^{31}P{^{1}H} NMR (d_6-DMSO, δ): 26.47, FT-IR spectrum (Zn–Se ATR, cm^{-1}): 1636 (C=O), 1591 (C=N). MS spectrum, *m*/*z*: calcd: 916.1012 found 917.0967 (M^++H). Anal calcd (%) for $C_{46}H_{37}N_4ClOP_2RuS$: C, 57.86; N, 9.69; H, 3.98; found: C, 57.91; N, 9.41; H, 3.93%.

Conflicts of interest

The authors have no known conflicts of interests to declare.

Acknowledgements

The authors wish to acknowledge the National Research Foundation (NRF-South Africa, DAAD), for the PhD bursary to NT, DST-National Research Foundation (SA) for the CPRR research grant to SO and DSI/Mintek Nanotechnology Innovation Centre for the research grant to MM.

References

1 P. Chinmay, *Results Chem.*, 2023, **6**, 101149.

2 S. Shirvalilou, Z. T. Parsaei, M. H. Parsaei, S. Sargazi, R. Sheervalilou, M. Shirvaliloo, H. Ghaznavi and S. Khoei, *Wiley Interdiscip. Rev.: Nanomed.*, 2023, e1922.

3 V. Voicu, F. M. Brehar, C. Toader, R.-A. Covache-Busuioc, A. D. Corlatescu, A. Bordeianu, H. P. Costin, B.-G. Bratu, L.-A. Glavan and A. V. Ciurea, *Biomolecules*, 2023, **13**, 1388.

4 L. De Michieli, M. D. Gaspari, G. Sinigiani, A. Lupi, L. Vedovelli, A. Salvalaggio, M. D. Barbera, S. Rizzo, K. Pilichou and D. Cecchin, *Int. J. Cardiol.*, 2023, **389**, 131204.

5 Y. Wang, Y. Hou, S. Wang, T. Zheng and W. Du, *ChemBioChem*, 2023, **24**, e202300395.

6 R. O. Omondi, D. Jaganyi and S. O. Ojwach, *BioMetals*, 2023, 1–15.

7 R. O. Omondi, A. O. Fadaka, A. A. Fatokun, D. Jaganyi and S. O. Ojwach, *J. Biol. Inorg. Chem.*, 2022, **27**, 653–664.

8 S. Kumar, M. K. Shukla, A. K. Sharma, G. K. Jayaprakash, R. K. Tonk, D. K. Chellappan, S. K. Singh, K. Dua, F. Ahmed and S. Bhattacharyya, *Med. Commun.*, 2023, **4**, e253.

9 J. J. Wilson and T. C Johnstone, *Curr. Opin. Chem. Biol.*, 2023, **76**, 102363.

10 Y. Zhang, B. T. Doan and G. Gasser, *Chem. Rev.*, 2023, **123**, 10135–10155.

11 R. O. Omondi, D. Jaganyi, S. O. Ojwach and A. A. Fatokun, *Inorg. Chim. Acta*, 2018, **482**, 213–220.

12 G. Sahu, S. A. Patra, S. Lima, S. Das, H. Görls, W. Plass and R. Dinda, *Chem.–Eur. J.*, 2023, **29**, e202202694.

13 R. K. Gupta, R. Pandey, G. Sharma, R. Prasad, B. Koch, S. Srikrishna, P.-Z. Li, Q. Xu, D. S. Pandey and . Inorg, *Chem*, 2013, **52**, 3687–3698.

14 T. E. Wood and A. Thompson, *Chem. Rev.*, 2007, **107**, 1831–1861.

15 G. H. Ribeiro, A. P. Guedes, T. D. de-Oliveira, C. R. de Correia, L. Colina-Vegas, M. A. Lima, J. A. Nobrega, M. R. Cominetti, F. V. Rocha and A. G. Ferreira, *Inorg. Chem.*, 2020, **59**, 15004–15018.

16 N. Alatrash, F. H. Issa, N. S. Bawazir, S. J. West, K. E. Van Manen-Brush, C. P. Shelor, A. S. Dayoub, K. A. Myers, C. Janetopoulos and E. A. Lewis, *Chem. Sci.*, 2020, **11**, 264–275.

17 S. Seyed Alinaghi, A. Karimi, H. Mojdeganlou, S. Alilou, S. P. Mirghaderi, T. Noori, A. Shamsabadi, O. Dadras, F. Vahedi and P. Mohammadi, *Sci. Rep.*, 2022, **5**, 13004–13018.

18 J. M. Rademaker-Lakhai, D. V.-D. Bongard, D. Pluim, J. H. Beijnen and J. H. Schellens, *Clin. Cancer Res.*, 2004, **10**, 3717–3727.

19 C. G. Hartinger, M. A. Jakupec, S. Zorbas-Seifried, M. Groessl, A. Egger, W. Berger, H. Zorbas, P. J. Dyson and B. K. Keppler, *Chem. Biodiversity*, 2008, **5**, 2140–2155.

20 A. K. Bytzek, G. Koellensperger, B. K. Keppler and C. G. Hartinger, *J. Inorg. Biochem.*, 2016, **160**, 250–255.

21 C. Scolaro, A. Bergamo, L. Brescacin, R. Delfino, M. Cocchietto, G. Laurenczy, T. J. Geldbach, G. Sava and P. J. Dyson, *J. Med. Chem.*, 2005, **48**, 4161–4171.

22 C. A. Vock, C. Scolaro, A. D. Phillips, R. Scopelliti, G. Sava and P. J. Dyson, *J. Med. Chem.*, 2006, **49**, 5552–5561.

23 R. E. Aird, *J. Cancer*, 2002, **86**, 1652–1657.

24 N. Alahmadi, H. S. Alhasan, H. Gomaa, A. A. Abdelwahab and M. Y. Emran, *RSC Med. Chem.*, 2022, **183**, 107909.

25 M. V. Babak, D. Plażuk, S. M. Meier, H. J. Arabshahi, J. Reynisson, B. Rychlik, A. Błauż, K. Szulc, M. Hanif and S. Strobl, *Chem.–Eur. J.*, 2015, **21**, 5110–5117.

26 P. Hikisz, E. Namiecińska, P. Paneth and E. Budzisz, *Molecules*, 2023, **28**, 3969.

27 N. K. Singh, Y. Kumar, R. P. Paitandi, R. K. Tiwari, A. Kumar and D. S. Pandey, *Inorg. Chim. Acta.*, 2023, **545**, 121241.

28 A. Alguacil, F. Scalambra, A. M. Romerosa-Nievas, A. Bento-Oliveira and F. Marques, *Bioinorg. Chem. Appl.*, 2023, **2023**, 15.

29 C. Chen, C. Xu, T. Li, S. Lu, F. Luo and H. Wang, *Eur. J. Med. Chem.*, 2020, **203**, 112605.

30 C. A. Annunziata, M. E. Cucciolito, M. D. Ronza, G. Ferraro, M. Hadiji, A. Merlino, D. Ortiz, R. Scopelliti, F. F. Tirani, P. J. Dyson and F. Ruffo, *Organometallics*, 2023, **42**, 952–964.

31 S. Nikolic, J. Arakelyan, V. Kushnarev, S. M. Alfadul, D. Stankovic and Y. I. Kraynik, *Inorg. Chem.*, 2023, **62**, 8188–8199.

32 T. S. Kamatchi, M. K. M. Subarkhan, R. Ramesh, H. Wang and J. G. Małecki, *Dalton Trans.*, 2020, **49**, 11385–11395.

33 A. Arunachalam, R. Rengan, D. Umapathy and J. V. Arockiam, *Organometallics*, 2022, **41**, 2474–2486.

34 C. Panda, A. Sarkar and S. S. Gupta, *Coord. Chem. Rev.*, 2020, **417**, 213314.

35 D. Bansal and R. Gupta, *Dalton Trans.*, 2016, **45**, 502–507.

36 P. Vijayan, S. Yadav, S. Yadav and R. Gupta, *Inorg. Chim. Acta*, 2020, **502**, 119285.

37 P. Vijayan, P. Viswanathamurthi, P. Sugumar, M. N. Ponnuswamy, M. D. Balakumaran, P. T. Kalaichelvan, K. Velmurugan, R. Nandhakumar and R. J. Butcher, *Inorg. Chem. Front.*, 2015, **2**, 620–639.

38 S. Biswas, S. Das, T. Gupta, S. K. Singh, M. Pissas and G. Rajaraman, *Chem.–Eur. J.*, 2016, **22**, 18532–18550.

39 S. R. I. Cooper, *CrystEngComm*, 2020, **22**, 7186.

40 A. M. Reilly, R. I. Cooper, C. S. Adjiman, S. Bhattacharya, A. D. Boese, J. G. Brandenburg, P. J. Bygrave, R. Bylsma, J. E. Campbell and R. Car, *Acta Crystallogr., Sect. B: Struct. Sci., Cryst. Eng. Mater.*, 2016, **72**, 439–459.

41 N. Muhammad, M. Hanif and P. Yang, *Coord. Chem. Rev.*, 2024, **499**, 215507.

42 T. S. Prathima, B. Choudhry, M. G. Ahmad, K. Chanda and M. M. Balamurali, *Coord. Chem. Rev.*, 2023, **490**, 215231.

43 R. O. Omondi and S. O. Ojwach, *Inorg. Chim. Acta*, 2020, **512**, 119883.

44 K. M. Oliveira, J. Honorato, G. R. Goncalves, M. R. Cominetti, A. A. Batista and R. S. Correa, *Dalton Trans.*, 2020, **49**, 12643–12652.

45 A. Zahirović, S. Roca, E. Kahrović and A. Višnjevac, *J. Mol. Struct.*, 2021, **1236**, 130326.

46 M. S. Alsaeedi, B. A. Babgi, M. H. Abdellattif, A. Jedidi, M. G. Humphrey and M. A. Hussien, *Molecules*, 2020, **26**, 76.

47 C.-V. Legna, W. Villarreal, M. Navarro, C. R. de Oliveira, A. E. Graminha, P. I. da, S. Maia, V. M. Deflon,

A. G. Ferreira, M. R. Cominetti and A. A. Batista, *J. Inorg. Biochem.*, 2015, **153**, 150–161.

48 P. O. Vardevanyan, A. P. Antonyan, M. A. Parsadanyan, H. G. Davtyan and A. T. Karapetyan, *Exp. Mol. Med.*, 2003, **35**, 527–533.

49 D. İnci, R. Aydin and Y. Zorlu, *Eur. Biophys. J.*, 2021, **50**, 771–785.

50 J. R Lakowicz and G. Weber, *Biochemistry*, 1973, **12**, 4161–4170.

51 M. Cory, D. D. Mckee, J. Kagan, D. W. Henry and J. A. Allen Miller, *J. Am. Chem. Soc.*, 1985, **107**, 2528–2536.

52 S. Kumar and M. S. Nair, *RSC Adv.*, 2021, **11**, 29354–29371.

53 M. Medjedović, A. R. Simovic, D. Ćoćić, M. Milutinović, L. Senft, S. Blagojević, N. Milivojević and B. Petrović, *Polyhedron*, 2020, **178**, 114334.

54 A. A. Adeleke, M. S. Islam, K. Olofinsan, V. F. Salau, C. Mocktar and B. Omondi, *New J. Chem.*, 2021, **45**, 17827–17846.

55 S. Balou, A. Zarkadoulas, M. Koukouvitaki, L. Marchiò, E. K. Efthimiadou and C. A. Mitsopoulou, *Bioinorg. Chem. Appl.*, 2021, 2021.

56 S. A. Elsayed, I. M. Elnabky, A. di Biase and A. M. El-Hendawy, *Appl. Organomet. Chem.*, 2022, **36**, e6481.

57 H. Edelhoch, *Biochem*, 1967, **6**, 1948–1954.

58 C. Kakoulidou, C. T. Chasapis, A. G. Hatzidimitriou, K. C. Fylaktakidou and G. Psomas, *Dalton Trans.*, 2022, 16688–16705.

59 S. Gurusamy, K. Krishnaveni, M. Sankarganesh, R. N. Asha and A. Mathavan, *J. Mol. Liq.*, 2022, **345**, 117045.

60 P. Y. Wang, C. T. Yang and L. K. Chu, *Chem. Phys. Lett.*, 2021, **781**, 138998.

61 K. L. Bell and H. C. Brenner, *Biochemistry*, 1982, **21**, 799–804.

62 M. M. Milutinović, A. Rilak, I. Bratsos, O. Klisurić, M. Vraneš, N. Gligorijević, S. Radulović and Ž. D. Bugarčić, *J. Inorg. Biochem.*, 2017, **169**, 1–12.

63 M. Ganeshpandian, R. Loganathan, E. Suresh, A. Riyasdeen, M. A. Akbarsha and M. Palaniandavar, *Dalton Trans.*, 2014, **43**, 1203–1219.

64 R. S. Correa, K. M. de Oliveira, F. G. Delolo, A. Alvarez, R. Mocelo, A. M. Plutin, M. R. Cominetti, E. E. Castellano and A. A. Batista, *J. Inorg. Biochem.*, 2015, **150**, 63–71.

65 T. Topală, A. Bodoki, L. Oprean and R. O. Radu, *Clujul Med.*, 2014, **87**, 215.

66 L. Fetzer, M. Ali, M. Xiangjun, J. P. Collin, C. Sirlin, C. Gaiddon and M. Pfeffere, *Dalton Trans.*, 2011, **40**, 8869–8878.

67 P. Hikisz, E. Namiecińska, P. Paneth and E. Budzisz, *Molecules*, 2023, **28**, 3969.